Figures and figure supplements

Forkhead transcription factor FKH-8 cooperates with RFX in the direct regulation of sensory cilia in *Caenorhabditis elegans*

Rebeca Brocal-Ruiz *et al*.

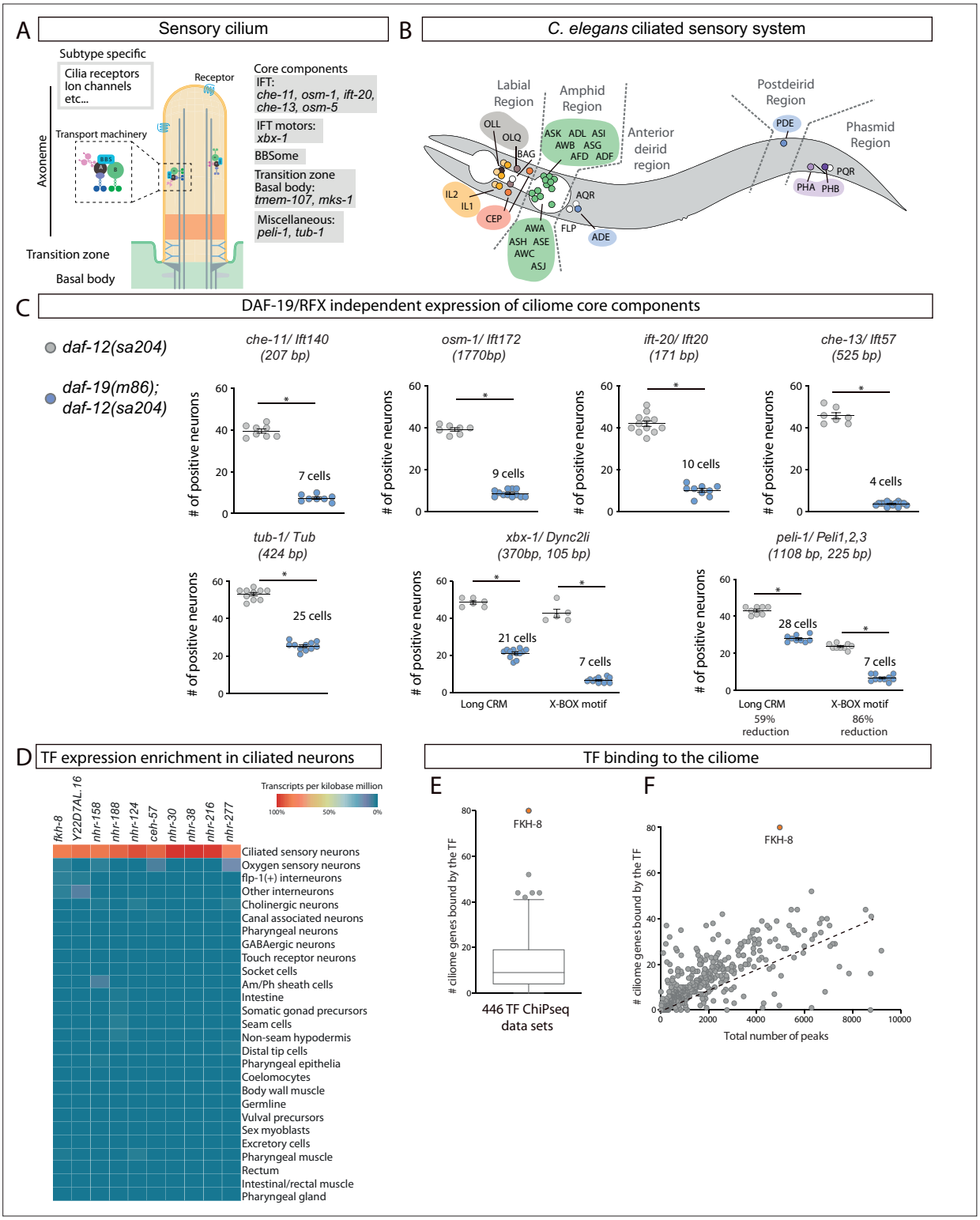

Figure 1. FKH-8 is a candidate for direct regulation of ciliome gene expression in *C. elegans*. (**A**) Schema for a sensory cilium. Cilia components (ciliome) can be divided into core and subtype-specific categories. Core genes whose reporters are analyzed in panel C and ***Figure 1—figure supplement 2*** are indicated by their function. (**B**) Lateral view of *C. elegans* hermaphrodite ciliated system. Sixty ciliated neurons from 25 different classes are distributed in five distinct anatomical regions. (**C**) Ciliome core components show persistent expression in double *daf-12(sa204); daf-19(m86)* mutants. The same extrachromosomal line was analyzed in the different genetic backgrounds. Each dot represents the total number of reporter-positive neurons in a single animal. Mean and standard error are represented. The mean number of remaining reporter-positive neurons in double *daf-12; daf-*

Figure 1 continued on next page

Figure 1 continued

19 mutants is indicated. Sample sizes for each genetic background: *che-11: n=8; osm-1: n≥7; ift-20: n≥9; che-13: n≥7; tub-1: n≥10; xbx-1: n≥5; peli-1: n≥8*. See ***Figure 1—source data 1*** for raw data and ***Figure 1—figure supplements 1 and 2*** for details on construct lengths and additional reporter scorings. (**D**) sc-RNA-seq data analysis identifies 10 TFs specifically enriched in ciliated sensory neurons. These TFs belong to FKH, ZF, NHR and HD families. See ***Figure 1—figure supplement 3*** for detailed description of TF expression in each ciliated neuron type. (**E**) ChIP-seq data analysis of 259 available TFs shows that FKH-8 ranks first in direct binding to regulatory regions assigned to the ciliome gene list. See ***Figure 1—source data 2*** for gene lists and ***Figure 1—figure supplement 3*** for core ciliome or subtype specific binding analysis. (**F**) Correlation of total number of peaks versus ciliome-gene peaks shows FKH-8 behaves as an outlier, demonstrating high binding to ciliome genes is not merely due to the high number of FKH-8 binding-events.

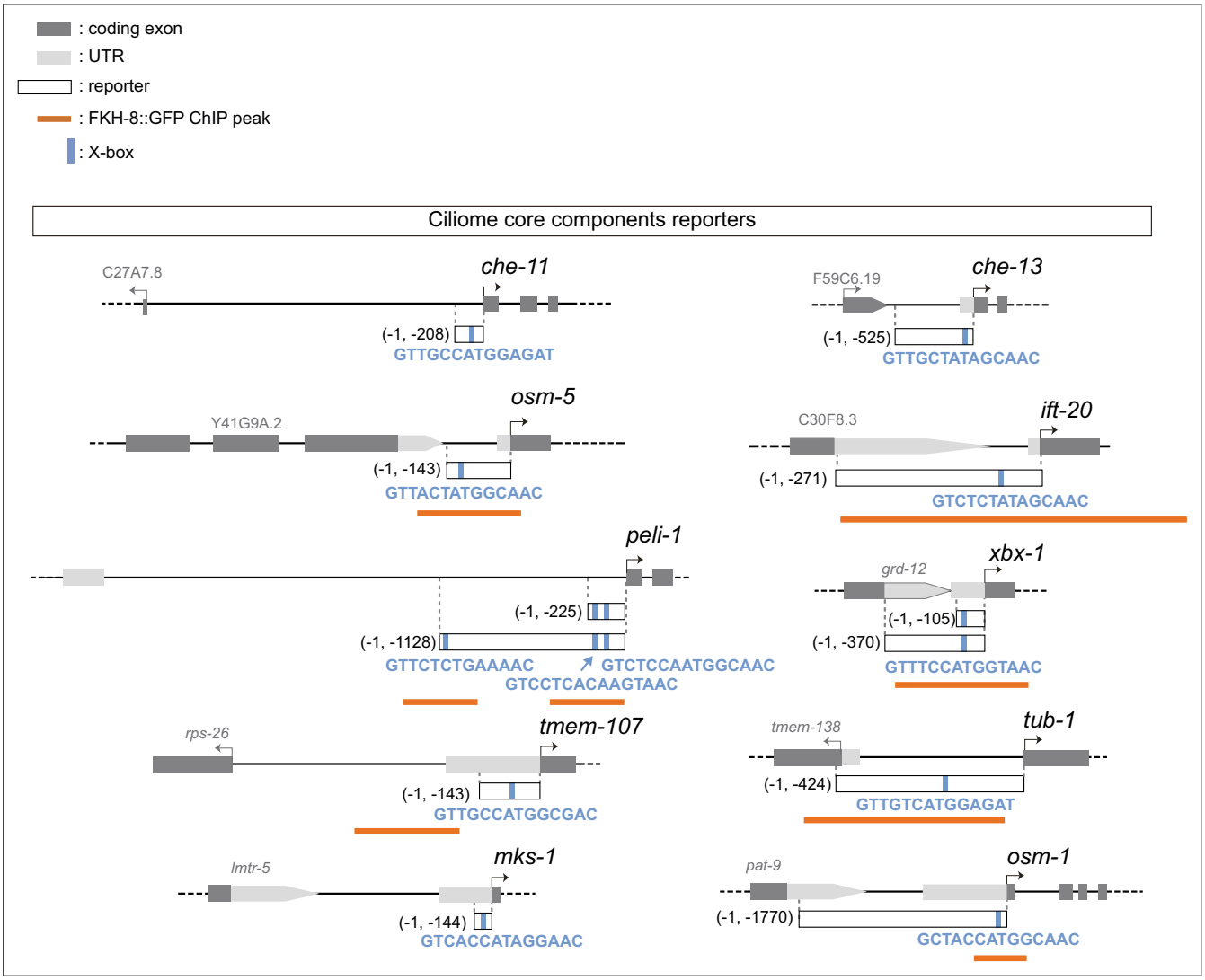

Figure 1—figure supplement 1. Ciliome reporters used in this work. Schematic representation of reporter constructs used in the manuscript. Selected core cilia components contain at least one experimentally validated X-box motif in their sequences (marked as a blue bar). For *che-11*, *che-13*, *osm5*, *ift-20*, *tub-1*, *mks-1* and *osm-1* see ***Efimenko et al., 2005***; for *peli-1* see ***Chu et al., 2012***, for *xbx-1* see ***Schafer et al., 2003***; for *tmem-107* see ***Lambacher et al., 2016***. Overlap between x-boxes and FKH-8 binding sites is found for *osm-5*, *ift-20*, *peli-1*, *xbx-1*, *tub1* and *osm-1*.

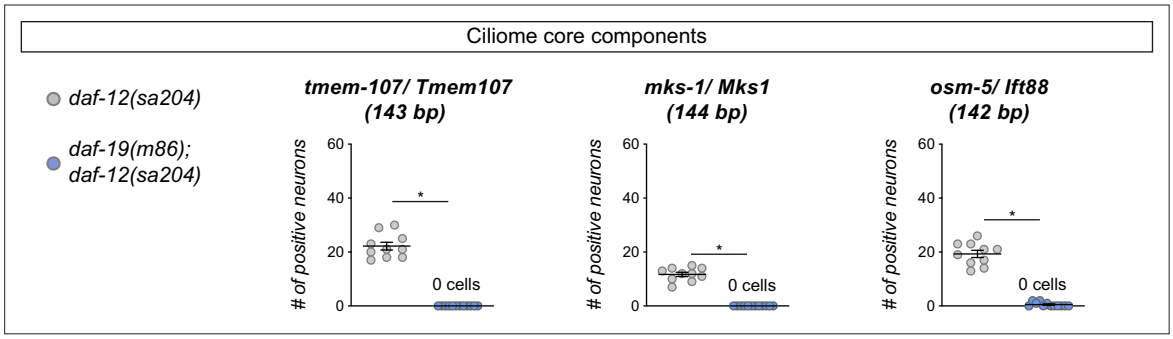

Figure 1—figure supplement 2. Reporter expression for some core ciliome genes is abolished in *daf-19(m86)* mutant. Expression of short reporters for the core cilia components *tmem-107*, *mks-1* and *osm-5* is completely abolished in *daf-12(sa204); daf-19(m86)* double mutants. The same extrachromosomal line was analyzed in the different genetic backgrounds. n≥10. Each dot represents the total number of reporter-positive neurons scored in a single animal. Mean and standard error are represented. See ***Figure 1—source data 1*** for raw scoring data.

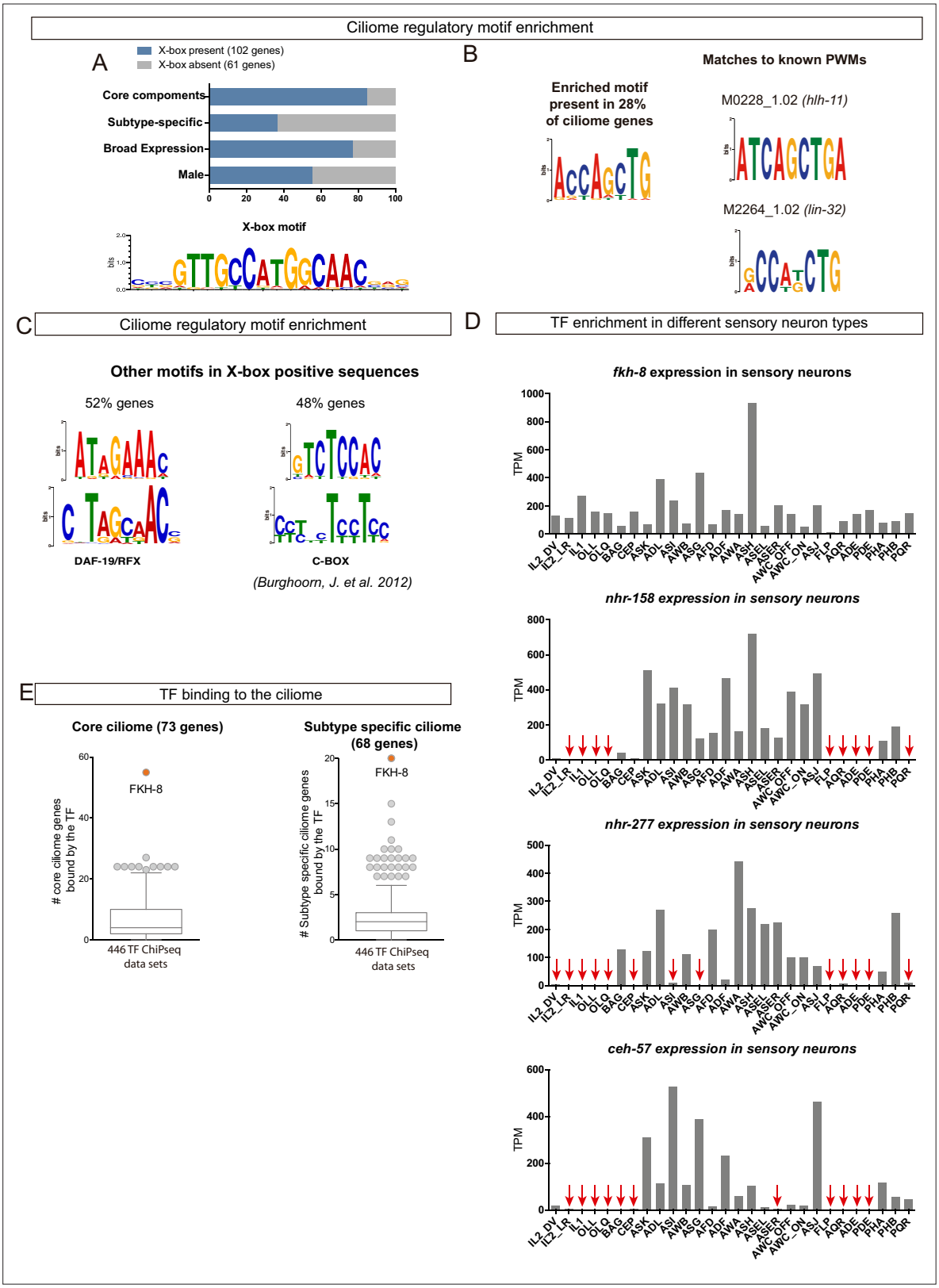

Figure 1—figure supplement 3. Available -omics data identifies FKH-8 as a candidate transcriptional regulator of ciliome genes in *C.elegans*. (**A**) DAF-19/RFX motifs (X-box) are enriched in regulatory sequences of core and broadly expressed ciliome genes more prominently than in subtype-specific features. Motif logo for the palindromic X-box motif. (**B**) De novo motif enrichment analysis of putative regulatory sequences of ciliome genes identifies a motif matching known binding site for the pro-neural bHLH TFs *lin-32* and *hlh-11*. (**C**) Two additional motifs enriched in regulatory sequences of

Figure 1—figure supplement 3 continued on next page

Figure 1—figure supplement 3 continued

ciliome genes containing X-box sites, show partial similarity to the DAF-19/RFX motif and to the ciliome-related motif C-BOX motif (***Burghoorn et al., 2012***). (**D**) sc-RNA-seq data of FACS-isolated neurons from L4 hermaphrodites (***Taylor et al., 2021***) show broad expression for *ceh-57*, *fkh-8*, *nhr-158* and *nhr-277* TFs across the whole ciliated system of *C. elegans*. Only *fkh-8* expression is detected in all ciliated neuron types. Red arrows indicate values lower than 10 TPM (transcripts per million). (**E**) ChIP-seq data analysis shows FKH-8 ranks first among 259 TFs directly binding to either core ciliome genes (left) or subtype-specific ciliary features (right).

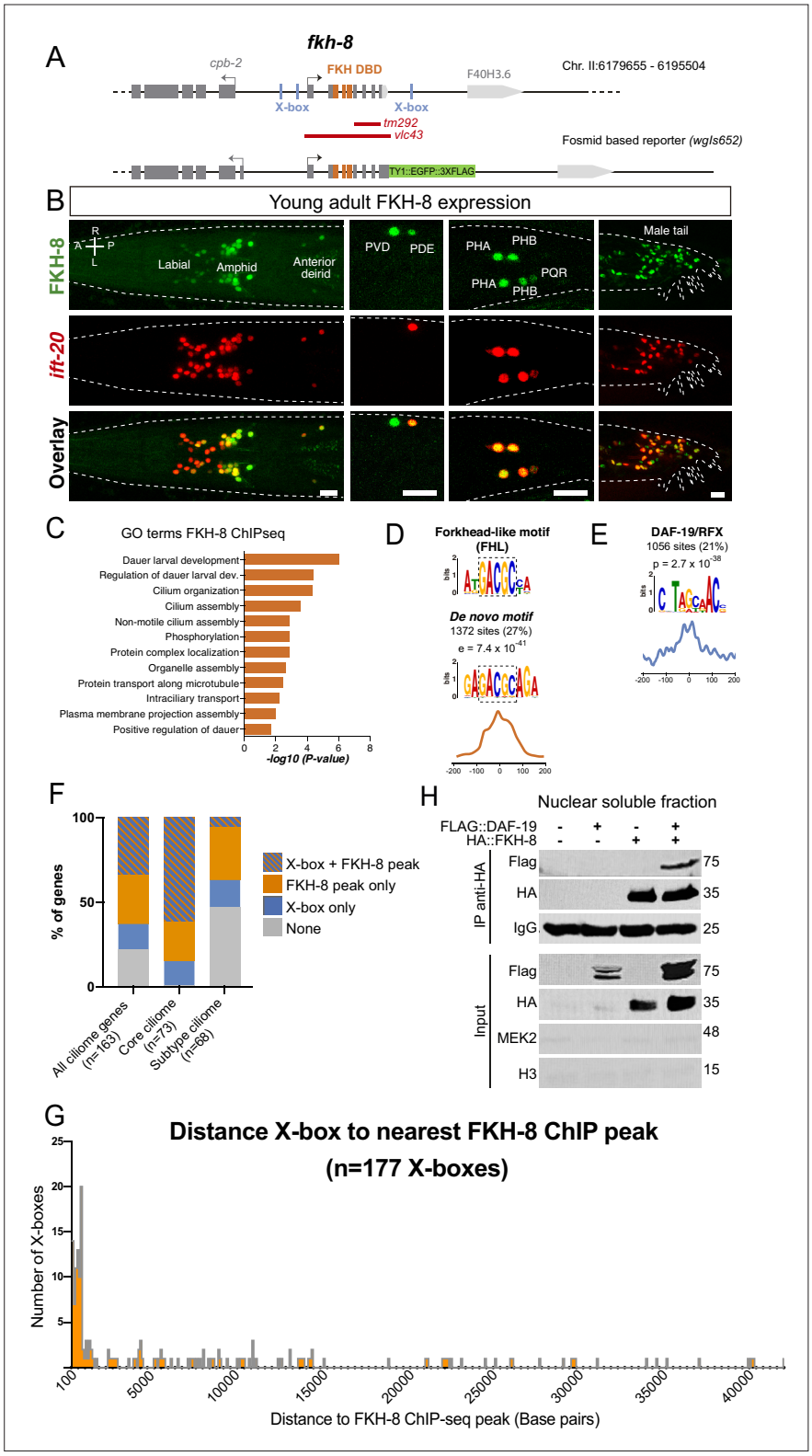

Figure 2. FKH-8 is expressed in sensory ciliated neurons, binds ciliome genes near DAF-19 X-boxes and physically interacts with DAF-19. (**A**) *fkh-8* locus (top) and fosmid based *fkh-8* reporter (bottom). Grey boxes represent exons and orange boxes correspond to exons coding for the FKH DNA binding domain (DBD). Putative *daf-19*/RFX binding sites (X-boxes) are depicted with blue lines. Red bars indicate extension for the corresponding deletion alleles. (**B**) Dorso-ventral views of young adult animals expressing both the fosmid-based FKH-8::GFP reporter

Figure 2 continued on next page

Figure 2 continued

(in green) and an integrated reporter for the panciliary marker *ift-20* (in red). A: anterior, P: posterior, R: right, L: left. Scale bar = 10 µm. See ***Figure 2—source data 1*** for quantification and ***Figure 2—figure supplement 1*** for embryonic expression patterns and expression correlation with DAF-19 and ciliome genes. (**C**) Genes associated to nearby FKH-8 binding events enrich Gene Ontology terms related to cilia regulated processes and/or functions. Data correspond to adjusted p-value. See ***Figure 2—source data 2*** for gene lists associated to GO terms (**D**) De novo motif analysis of FKH-8 ChIP-seq data identifies a motif present in 27% of peaks, enriched at central positions, that matches a Forkhead like (FHL) motif. (**E**) DAF-19/RFX binding motifs (PWM M1534_1.02) are present in 21% of the FKH-8 bound regions and are enriched at central positions. See ***Figure 2—figure supplement 2*** for similar analysis on additional FKH ChIP-seq data sets. (**F**) Distribution of ciliome genes in four different categories: (1) genes with both X-box motifs and FKH-8 binding events; (2) genes with only FKH-8 binding; (3) Genes with X-box motifs only and (4) Genes with neither FKH-8 binding or X-boxes. Most ciliome genes contain both X-boxes and FKH-8 peaks, this dual signature is highly prevalent in core ciliome genes while is minoritary in subtype ciliome genes. See ***Figure 2—source data 2*** for gene lists associated to each signature. (**G**) Distance between X-boxes found in ciliome genes and the center of the nearest FKH-8 ChIP-seq peak. 42% of X-boxes are located less than 600 bp from a FKH-8 ChIP-seq peak. See ***Figure 2—figure supplement 2*** for differential analysis of core and subtype ciliome genes. (**H**) Co-immuno precipitation of HA tag FKH-8 and FLAG tag DAF-19 expressed in HEK293 cells shows physical interaction between both transcription factors in the soluble fraction of nuclear extracts. MEK2 is used to assess for the presence of cytoplasmic components and Histone H3 to assess the presence of chromatin. See ***Figure 2—source data 3*** for original blots and ***Figure 2—figure supplement 2*** for additional analysis of interaction in chromatin associated fractions.

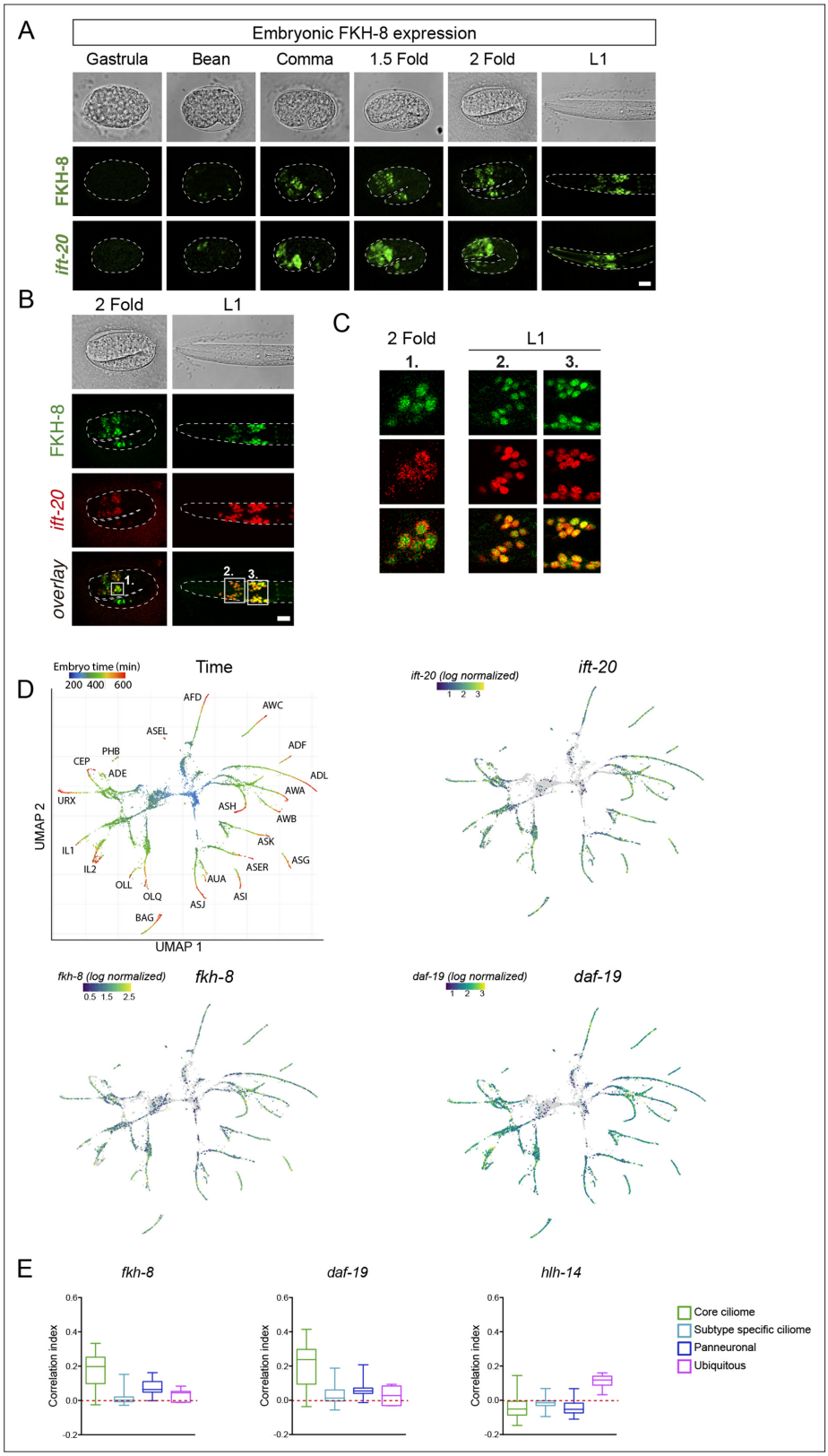

Figure 2—figure supplement 1. *fkh-8* expression along ciliated system development. (**A**) Representative Z projections of developmental embryonic milestones until hatching (**L1**) shows FKH-8::GFP fosmid reporter expression matches in time and space panciliary reporter *ift-20::gfp* expression. Scale bar = 10 µm. (**B**) Representative Z projections of two fold embryo and fist larval stage (**L1**) animals expressing both FKH-8::GFP

Figure 2—figure supplement 1 continued on next page

Figure 2—figure supplement 1 continued

fosmid reporter (in green) and an integrated reporter for the panciliary marker *ift-20:: tagRFP* (in red). Note that due to long maturation time of the tag-RFP reporter, *ift-20::tagRFP* expression is only detected from the two fold stage, while *ift-20::gfp* reporter in (**A**) is first detected at bean stage, similar to *fkh-8* expression. Scale bar = 10 µm. (**C**) Single Z-plane from regions indicated in (**B**) show colocalization of FKH-8::GFP and RFP in the ciliated sensory neurons. (**D**) Embryonic sc-RNA-data (***Packer et al., 2019***) from *C. elegans* ciliated neurons and their progenitor cells. Pseudo-time (left pannel) shows the maturation trajectory of ciliated neurons that coincides with increasing *ift-20*, *fkh-8,* and *daf-19* expression. (**E**) Correlation index of *fkh-8, daf-19* and *hlh-14* TF scRNAseq expression and four different gene categories (core ciliome, subtype ciliome, panneuronal or ubiquitous) in all ciliated lineages (***Packer et al., 2019***). *fkh-8* and *daf-19* expression shows high correlation index with core ciliome genes but not with other gene categories, while *hlh-14,* bHLH TF not involved in ciliogenesis shows low correlation values in all categories. See ***Figure 2—source data 2*** f for raw data.

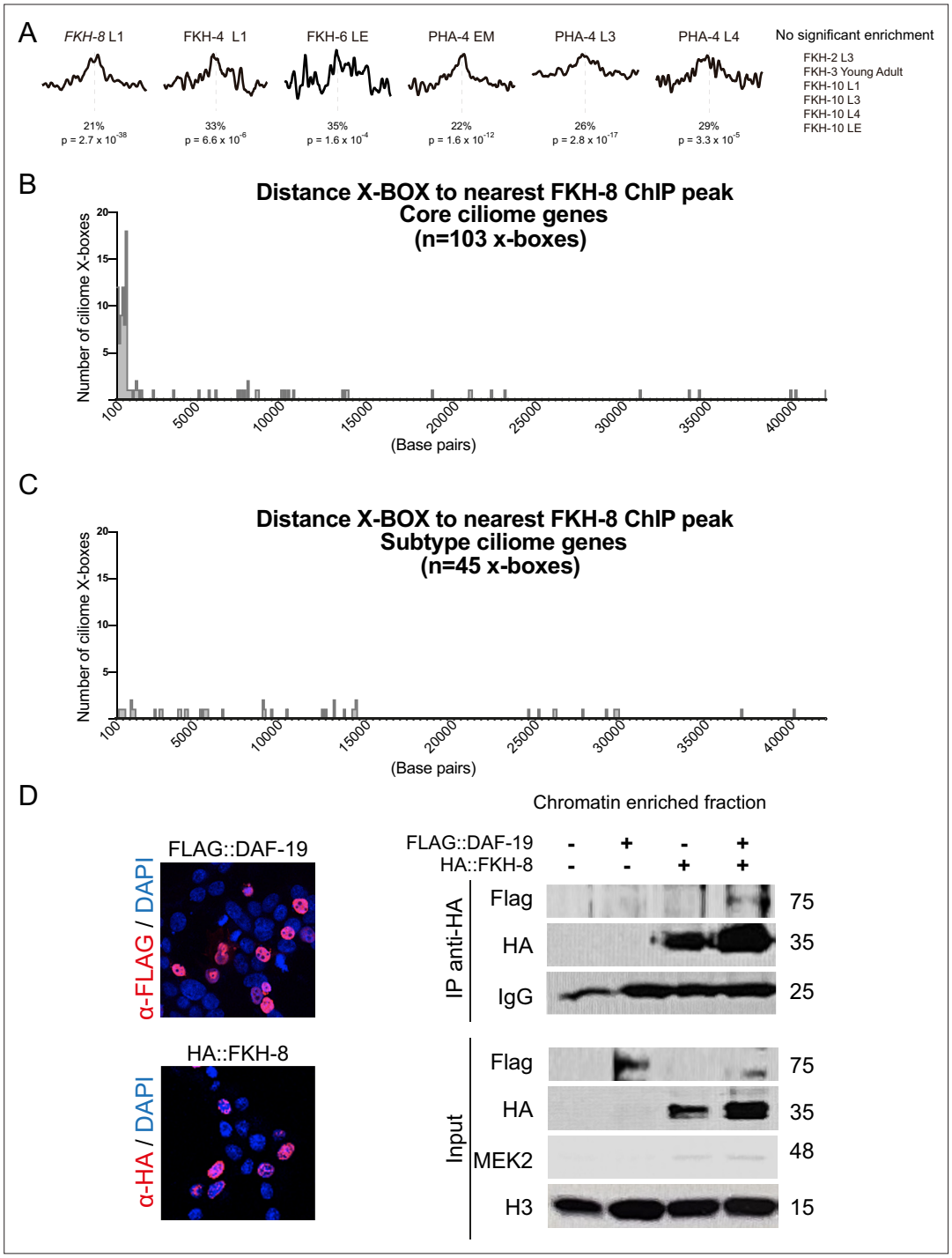

Figure 2—figure supplement 2. FKH-8 binds near X-BOX motifs. (**A**) Analysis of DAF-19/RFX binding motifs (PWM M1534_1.02) in peaks for ChIP-seq datasets of other *C. elegans* FKH TFs present in ENCODE database. There is no significant enrichment for DAF-19 motif in FKH-2, FKH-3, and FKH-10 datasets. Motif enrichment in FKH-4, FKH-6, and PHA-4 datasets is less significant and shows less defined enrichment in the centre of the peaks. p represents p Value associated to motif enrichment and % refers to the number of peaks with the motif present. EM: Embryo mixed stage; L1: Larval stage 1; L3: Larval stage 3, L4: Larval stage 4, LE: Late embryo. See ***Figure 2—source data 2*** for detailed data. (**B**) Distance between X-boxes found in the promoter regions of core ciliome genes and the center of the nearest FKH-8 ChIP peak. 63% of X-boxes are located less than 600 bp from a FKH-8 ChIP peak. (**C**) Distance between X-boxes found in the promoter regions of subtype ciliome genes and the center of the nearest FKH-8 ChIP peak. 9% of X-boxes are located less than 600 bp from a FKH-8 ChIP peak. (**D**) Co-

Figure 2—figure supplement 2 continued on next page

Figure 2—figure supplement 2 continued

immuno precipitation of FKH-8 and DAF-19 expressed in HEK293 cells. Micrographs shows nuclear localization of transfected HA::FKH-8 and FLAG::DAF-19. In addition to the interaction detected in the soluble nuclear fraction (***Figure 2***), both factors also interact bound to DNA (chromatin fraction). See ***Figure 2—figure supplement 2—source data 1*** for original blots.

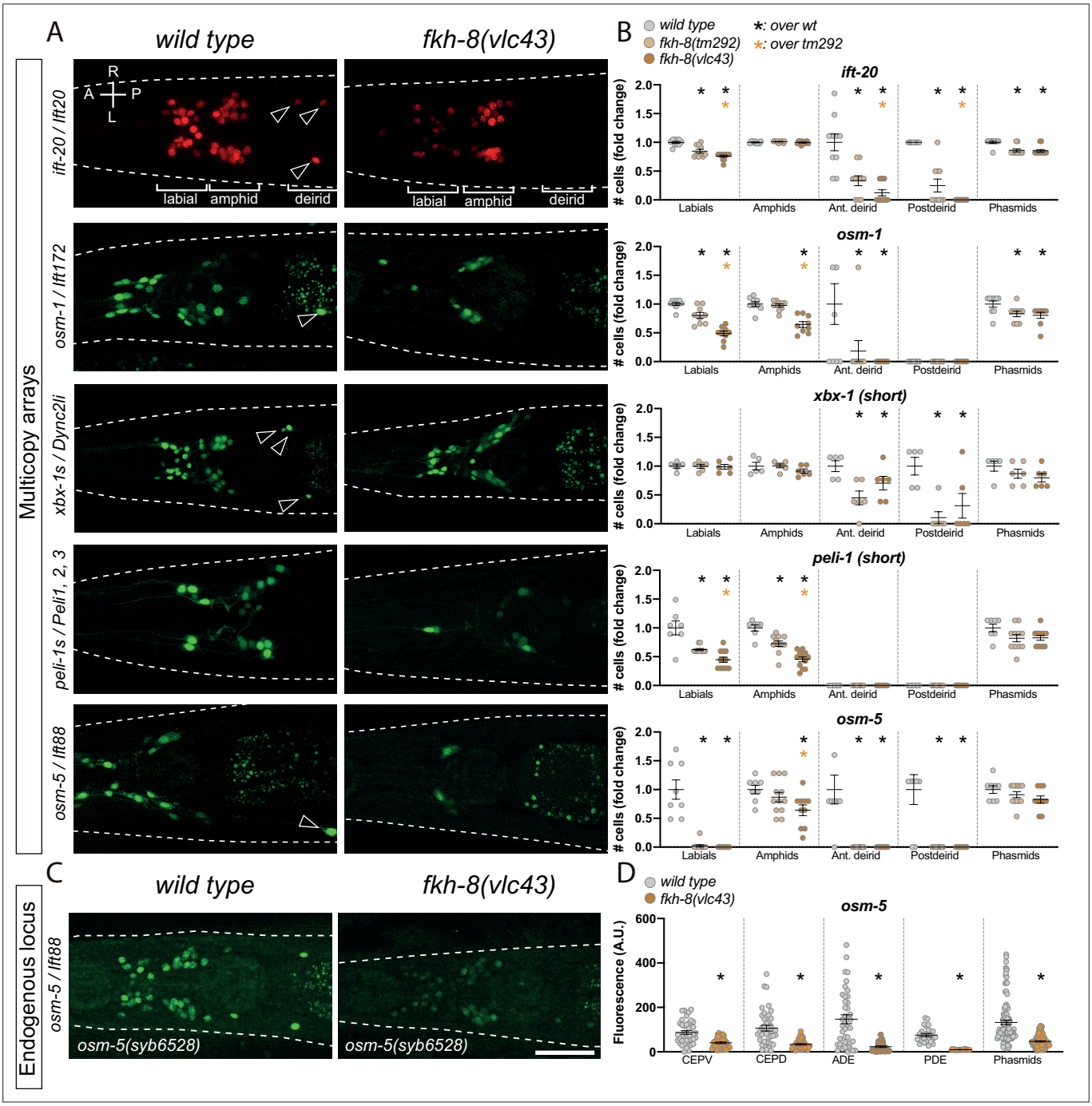

Figure 3. FKH-8 TF and FKH-binding sites are required for correct core ciliome gene reporter expression. (**A**) Dorso-ventral images from young adult heads expressing different core ciliome multicopy array gene reporters in *wild type* and *fkh-8(vlc43)* null mutant animals. All reporters are extrachromosomal arrays except for *ift-20* reporter which is integrated. Arrow heads point deirid expression lost in the mutant. A: anterior, P: posterior, R: right, L: left. (**B**) Quantification of the number of *gfp*-positive cells in five distinct anatomical regions for each reporter in *wild type, fkh-8(tm292)* hypomorphic allele and *fkh-8(vlc43)* null mutant. To facilitate comparisons, values in each region are normalized to controls. The same extrachromosomal line was analyzed in the different genetic backgrounds. Each dot represents the number of reporter-expressing neurons scored in a single animal. Mean and standard error are represented. Black asterisk denotes significantly different from *wild type* and orange asterisk indicates *vlc43* is significantly different from *tm292* allele. Sample sizes for each genetic background: *ift-20: n≥10; osm-9: n=9; osm-5: n≥8; peli-1: n≥7; xbx-1: n≥5.* See ***Figure 3—source data 1*** for raw scoring data, ***Figure 3—figure supplement 1*** for analysis of the hypomorphic recessive nature of the *tm292* allele and quantification of additional reporters not affected in *fkh-8* mutants, see ***Figure 3—figure supplement 2*** and ***Figure 3—source data 2*** for functional characterization of predicted FKH binding sites in *ift-20* and *xbx-1* regulatory regions. (**C**) Dorso-ventral images from young adult heads expressing *GFP* from the endogenously tagged *osm-5* locus *[osm-5(syb6528), osm-5::SL2::GFP::H2B]* in *wild type* and *fkh-8(vlc43)* null mutant. A global decrease

Figure 3 continued on next page

Figure 3 continued

in fluorescence intensity is detected in *fkh-8(vlc43)* animals compared to *wild type*. Scale bar = 25 µm. (**D**) Fluorescence intensity level quantification in specific ciliated neuron populations shows significant reduction of expression in *fkh-8(vlc43)* animals. A. U.: arbitrary units. See ***Figure 3—source data 1*** for raw scoring data. n≥*20* for each cell type and genetic background.

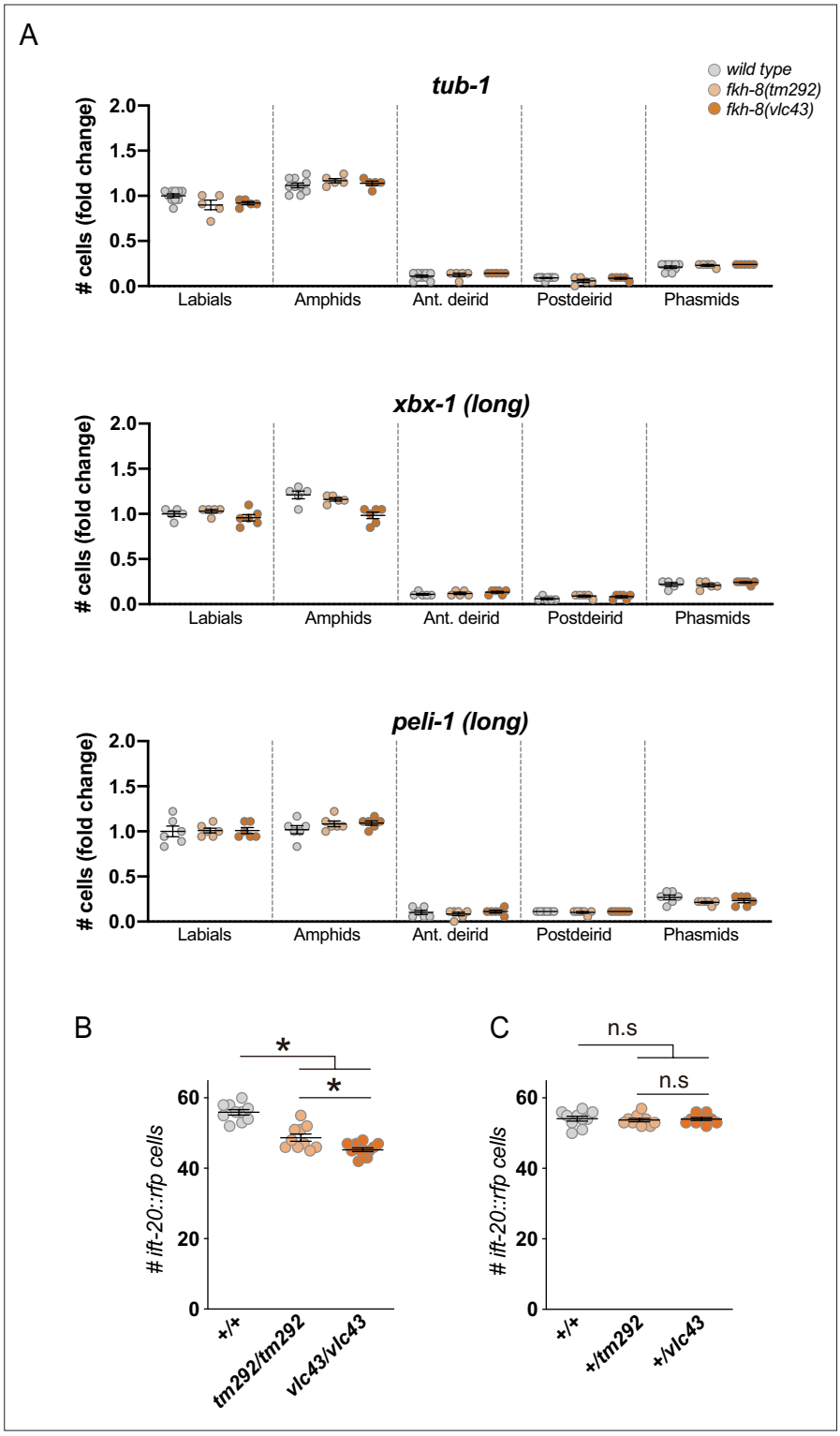

Figure 3—figure supplement 1. *f. fkh-8(tm292)* is a hypomorphic recessive allele. (**A**) Quantification of the number of *gfp*-positive cells in five distinct anatomical regions for each reporter in *wild type, fkh-8(tm292)* hypomorphic allele and *fkh-8(vlc43)* null mutant. To facilitate comparisons, values in each region are normalized to controls. The same extrachromosomal line was analyzed in the different genetic backgrounds. Each dot represents the number of reporter-expressing neurons scored in a single animal. Mean and standard error are represented. *fkh-8(tm292)* and *fkh-8(vlc43)* show similar expression values than wild type for these markers. See ***Figure 3—source data 1*** for raw scoring data. (**B**) Quantification of the number of *ift-20::rfp*-positive cells in *wild type, fkh-*

Figure 3—figure supplement 1 continued on next page

Figure 3—figure supplement 1 continued

8(tm292) and *fkh-8(vlc43)* mutants shows stronger defects in *vlc43* null allele.: $n \geq 5$. (**C**) Heterozygote cross progeny from *wild type*, *fkh-8(tm292)* and *fkh-8(vlc43)* show similar number of *ift-20::rfp*-positive cells denoting the recessive nature of both alleles. $n \geq 10$.

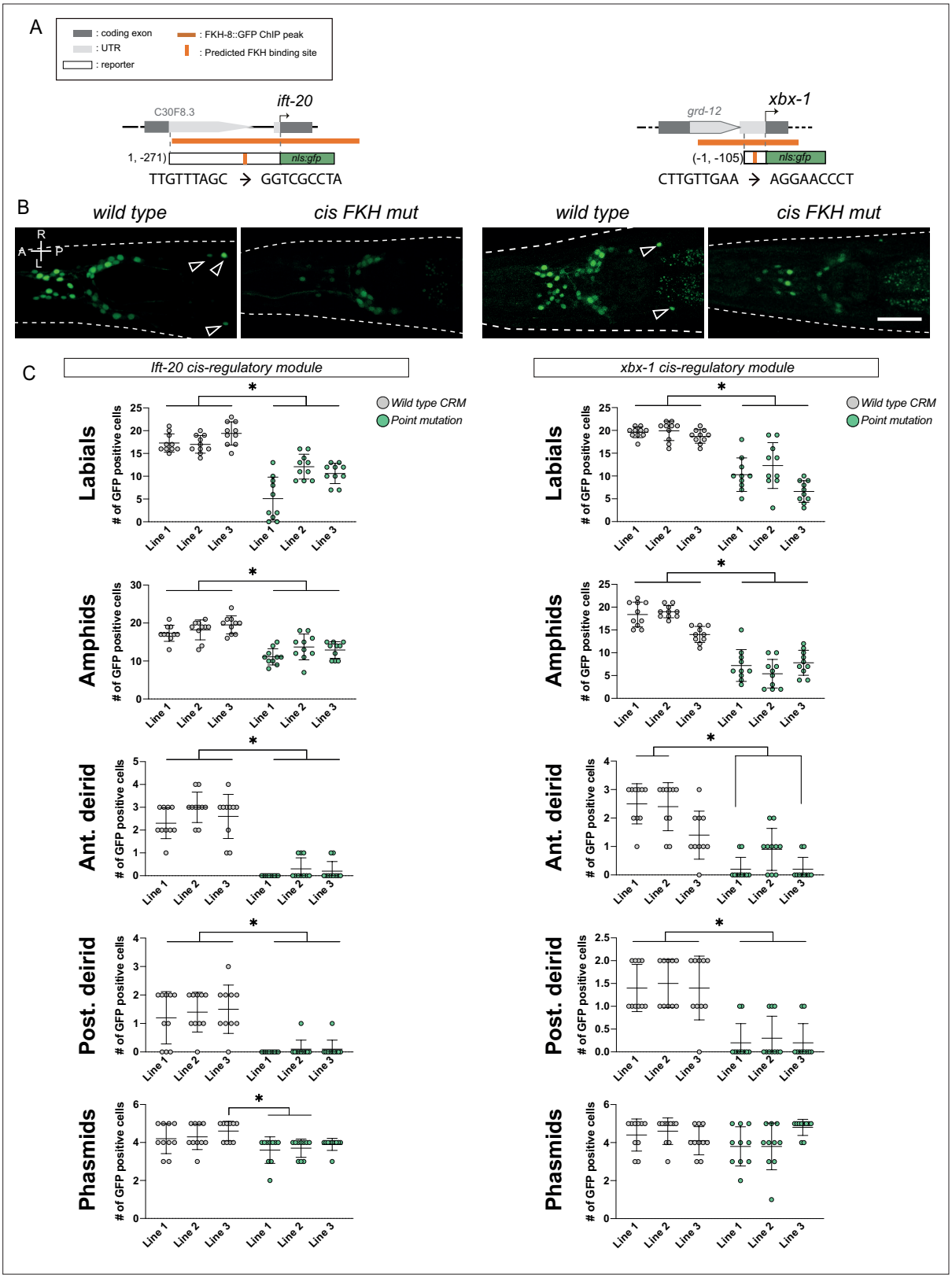

Figure 3—figure supplement 2. *f.* Functional characterization of putative FKH sites in cis-regulatory modules of two core ciliome components. (**A**) Schematics for the *ift-20* and *xbx-1* loci and reporters. Dark grey boxes represent exons whereas light grey boxes correspond to UTRs. FKH-8 Chip-seq peaks are depicted with an orange horizontal line while predicted FKH DNA binding motifs are indicated with a vertical orange bar. Sequences corresponding to *wild type* and mutated putative FKH sites are indicated. See ***Figure 3—source data 2*** for FKH putative binding site assignment.

Figure 3—figure supplement 2 continued on next page

Figure 3—figure supplement 2 continued

(**B**) *Cis*-regulatory mutation of putative FKH sites greatly reduces ciliome gene reporter expression. Representative dorso-ventral images from young adult heads expressing *wild type* or FKH-site-mutated reporters for core ciliome genes *ift-20* (left) and *xbx-1* (right). A: anterior, P: posterior, R: right, L: left. Scale bar = 25 µm. (**C**) Quantification of total number of *gfp*-positive cells for *wild type* and point mutated *gfp* reporters. Each graph represents one of the five anatomical regions scored. Three different extrachromosomal lines were analyzed for each construct. Each dot represents the number of reporter-expressing neurons scored in a single animal. Statistically significant differences are indicated with asterisks. See ***Figure 3—source data 1*** for raw scoring data. n=10.

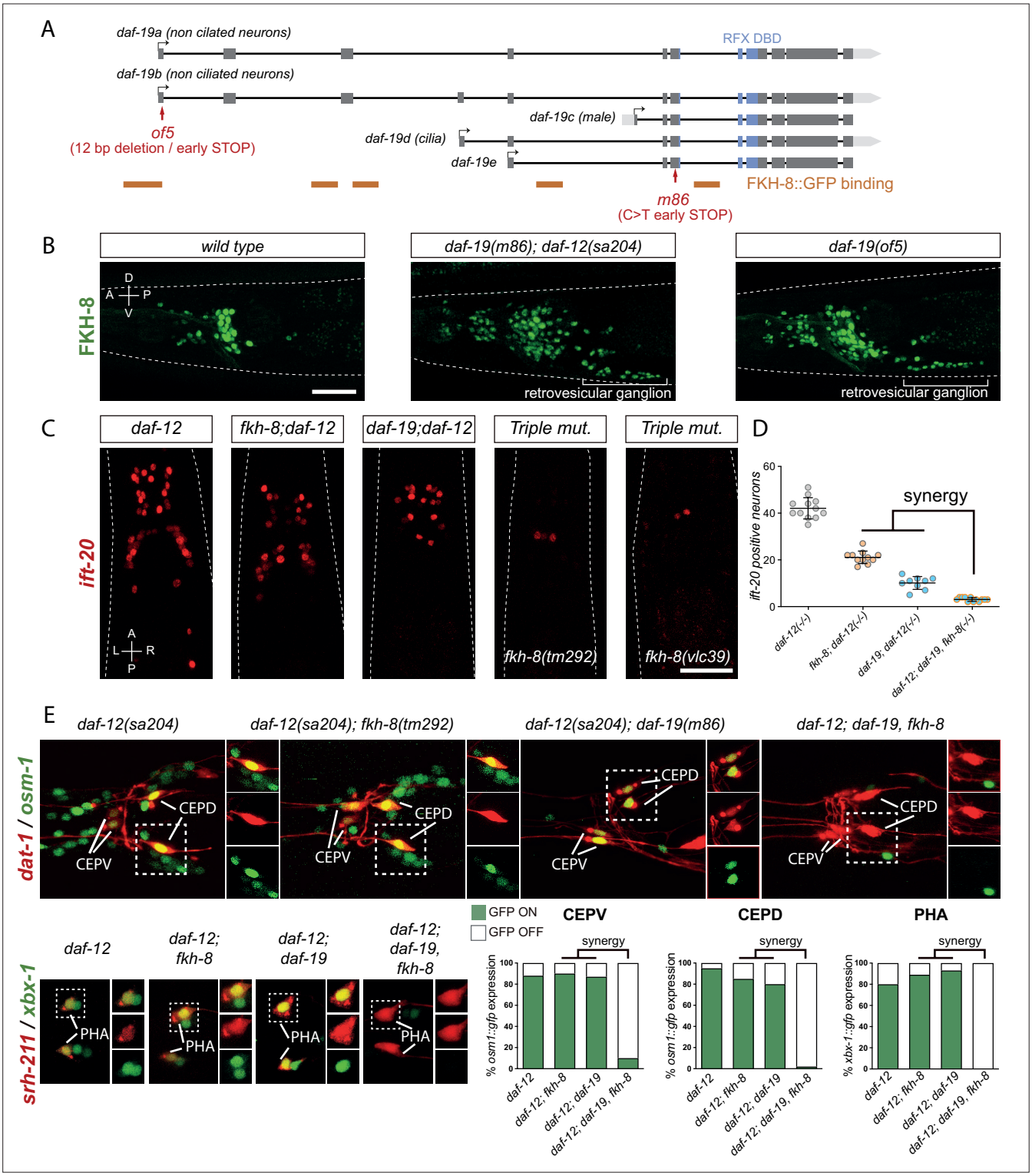

Figure 4. FKH-8 and DAF-19 exhibit crosstalk and synergistic effects in the transcriptional regulation of ciliome genes. (**A**) *daf-19* locus codes for five different *daf-19* isoforms. Grey boxes represent exons whereas blue boxes correspond to exons coding for the RFX DNA binding domain (DBD). FKH-8 binding events are depicted as orange lines. Red arrows locate mutations of the corresponding alleles. (**B**) Lateral views from young adult hermaphrodite heads expressing *fkh-8* fosmid-based reporter (*wgIs652*). Lack of all *daf-19* isoforms (*m86* allele) derepresses *fkh-8* in non-ciliated neurons. This phenotype is mimicked by the specific absence of long *daf-19a/b* isoforms (*of5* allele). Scale bar = 25 µm. See ***Figure 4—figure supplement 1*** for unaffected DAF-19 expression in ciliated neurons in *fkh-8(vlc43)* mutants. (**C**) Dorso-ventral images from young adult hermaphrodites showing core ciliome *ift-20* reporter expression in different genetic backgrounds. Scale bar = 25 µm. (**D**) Mean number of *ift-20* reporter-expressing

Figure 4 continued on next page

Figure 4 continued

neurons in *daf-12(sa204); daf-19(m86)*, *fkh-8(tm292)* triple mutants is significantly different from each of the double mutants and significantly lower than the expected from the multiplicative effect of both *daf-12(sa204); fkh-8(tm292)* and *daf-12(sa204); daf-19(m86)* animals. The same extrachromosomal line was analyzed in the different genetic backgrounds. Each dot represents the number of reporter-expressing neurons scored in a single animal. Mean and standard error are represented. See ***Figure 4—figure supplement 2*** for quantification of FKH-8 and DAF-19 synergistic effects in *xbx-1* and *peli-1* reporter expression and ***Figure 4—source data 1*** for raw data and statistics for all analyzed genetic backgrounds. n≥*10* for each genetic background. (**E**) Analysis of *osm-1* and *xbx-1* ciliome reporters in specific subpopulations of ciliated neurons. CEPV and CEPD are labeled with *dat-1::mcherry (otIs181) and srh-211:: tagRFP (vlcEx1365)* is expressed in PHA neuron, both reporters are unaffected in all genetic backgrounds. Quantification of ciliome reporters is depicted in the corresponding graphs. ***Figure 4—source data 1*** for raw data and statistics for all analyzed genetic backgrounds, n=30 worms per genotype and reporter construct.

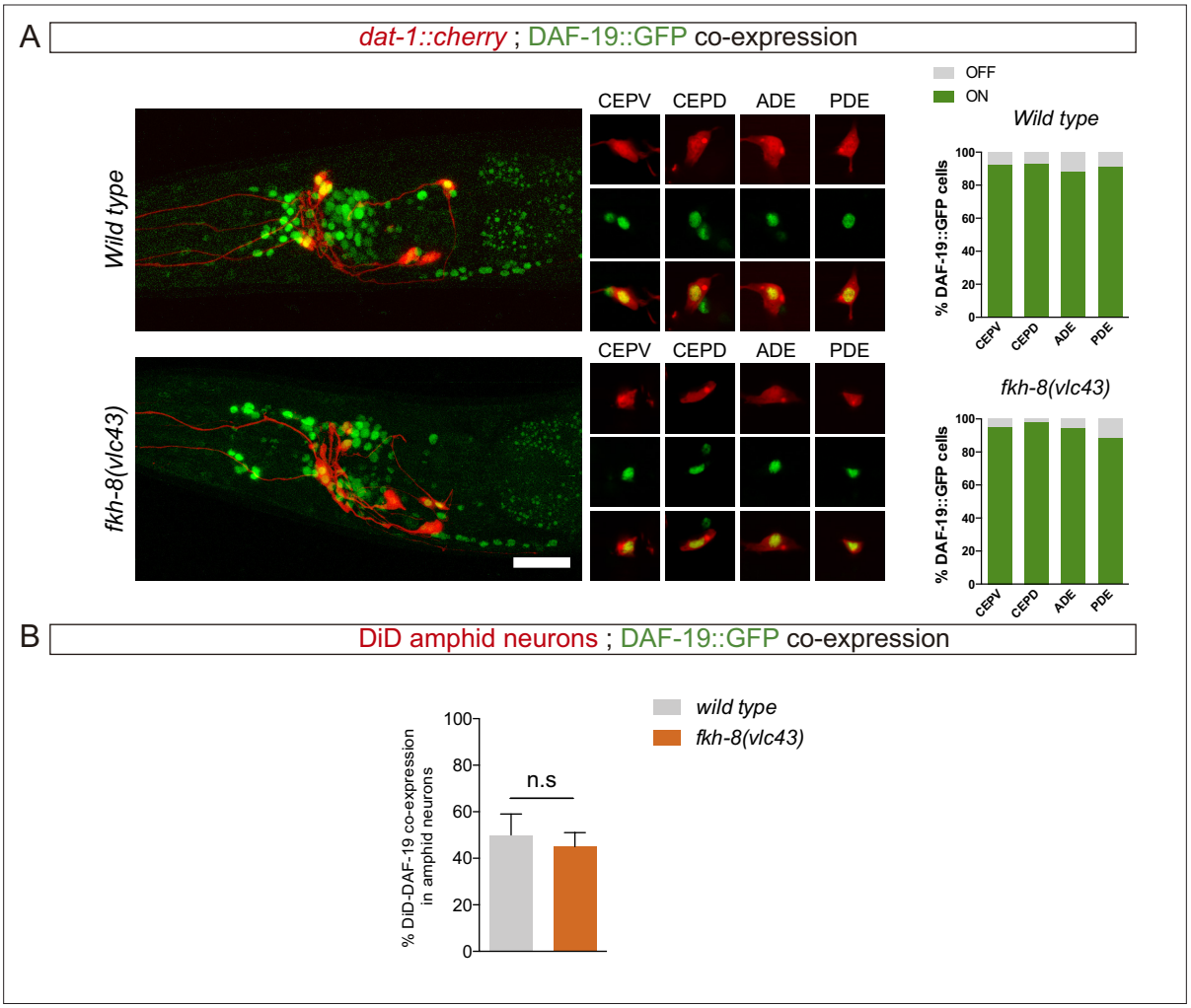

Figure 4—figure supplement 1. Lack of FKH-8 has no major effect on DAF-19 expression. (**A**) Representative lateral views from heads of young adult hermaphrodites co-expressing a fosmid-based DAF-19::GFP reporter and *dat-1::mcherry* reporter labeling the dopaminergic neurons. Lack of FKH-8 does not affect DAF-19::GFP expression pattern. Co-localization analysis shows normal expression in the dopaminergic ciliated neurons (CEPV, CEPD, ADE, PDE), quantified in the graphs. Scale bar = 20 µm. See ***Figure 4—source data 1*** for raw data. N=50. (**B**) *daf-19* expression is largely unaffected in the subpopulation of DiD-positive ciliated amphid neurons in null *fkh-8* mutant animals. DAF-19::GFP is consistently detected in the ASI, ADL and AWB neurons in both *wild type* and null *fkh-8* mutant backgrounds. Mean and standard deviation are represented. n=10 animals.

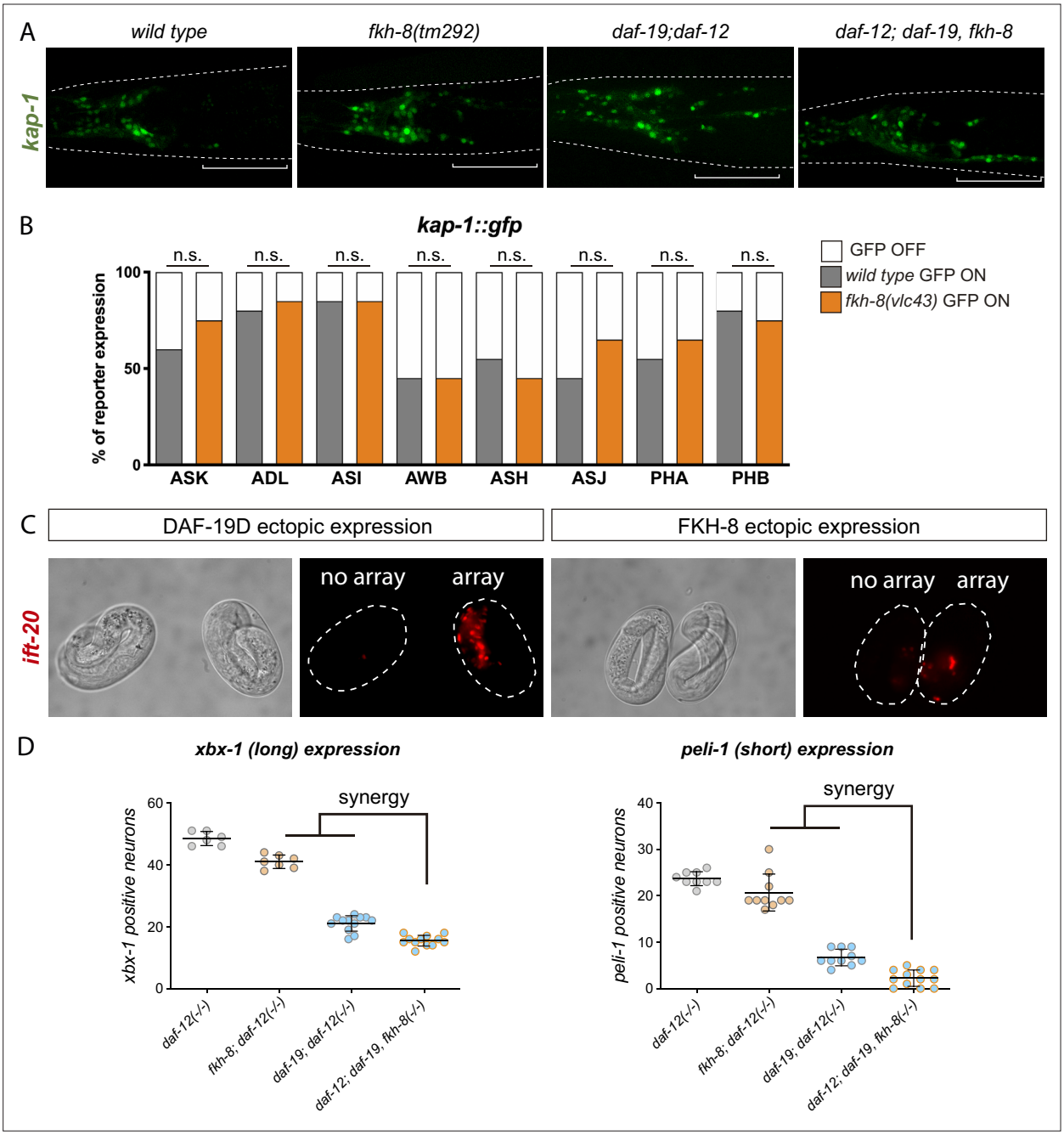

Figure 4—figure supplement 2. FKH-8 and DAF-19 show synergistic effects in the transcriptional regulation of the ciliome. (**A**) Representative micrographs of *kap-1* reporter expression in different genetic backgrounds. *kap-1::gfp* is unaffected in *fkh-8(tm292)* and ectopically expressed both in *daf-19(m86); daf-12(sa204)* and *daf-12(sa204); daf-19(m86), fkh-8(tm292)*. Ectopic expression is more evident in the posterior part of the head, labeled with a white line. (**B**) Quantification of *kap-1* reporter expression in different subpopulations of sensory ciliated neurons shows similar expression in *fkh-8(vlc43)* null mutants and *wild type* animals. N≥19. (**C**) Representative micrographs of embryonic *ift-20::rfp* expression after ectopic expression of DAF-19D and FKH-8 through a heatshock inducible promoter. Two-cell stage embryos were grown at 20 °C for 4 hours and then heat shocked at 37 °C for 20 min, embryos were scored for ectopic *ift-20::rfp* 20 hours after heatshock. Two different lines were analyzed for each construct. 100% of embryos with DAF19D ectopic expression show ectopic *ift-20::rfp* expression, while heatshocked embryos without array had normal *ift-20::rfp* expression (Line 1 n=24 embryos with array, n=11 embryos without array; Line 2 n=21 embryos with array, n=12 embryos without array). Ectopic FKH-8 expression had no obvious effect on *ift-20::rfp*. (Line 1 n=10 embryos with array, n=5 embryos without array; Line 2 n=15 embryos with array, n=3 embryos without array). (**D**) Quantification of ciliome reporters in *fkh-8* and *daf-19* mutants. The same extrachromosomal line was analyzed in the different genetic backgrounds. Each dot represents the number of reporter-expressing neurons scored in a single animal. Mean and standard error are represented. For both reporters, triple mutant is significantly different from each of the double mutants and significantly lower than the expected from the multiplicative effect of both *daf-12(sa204); fkh-8(tm292)* and *daf-12(sa204); daf-19(m86)* animals. n≥6.

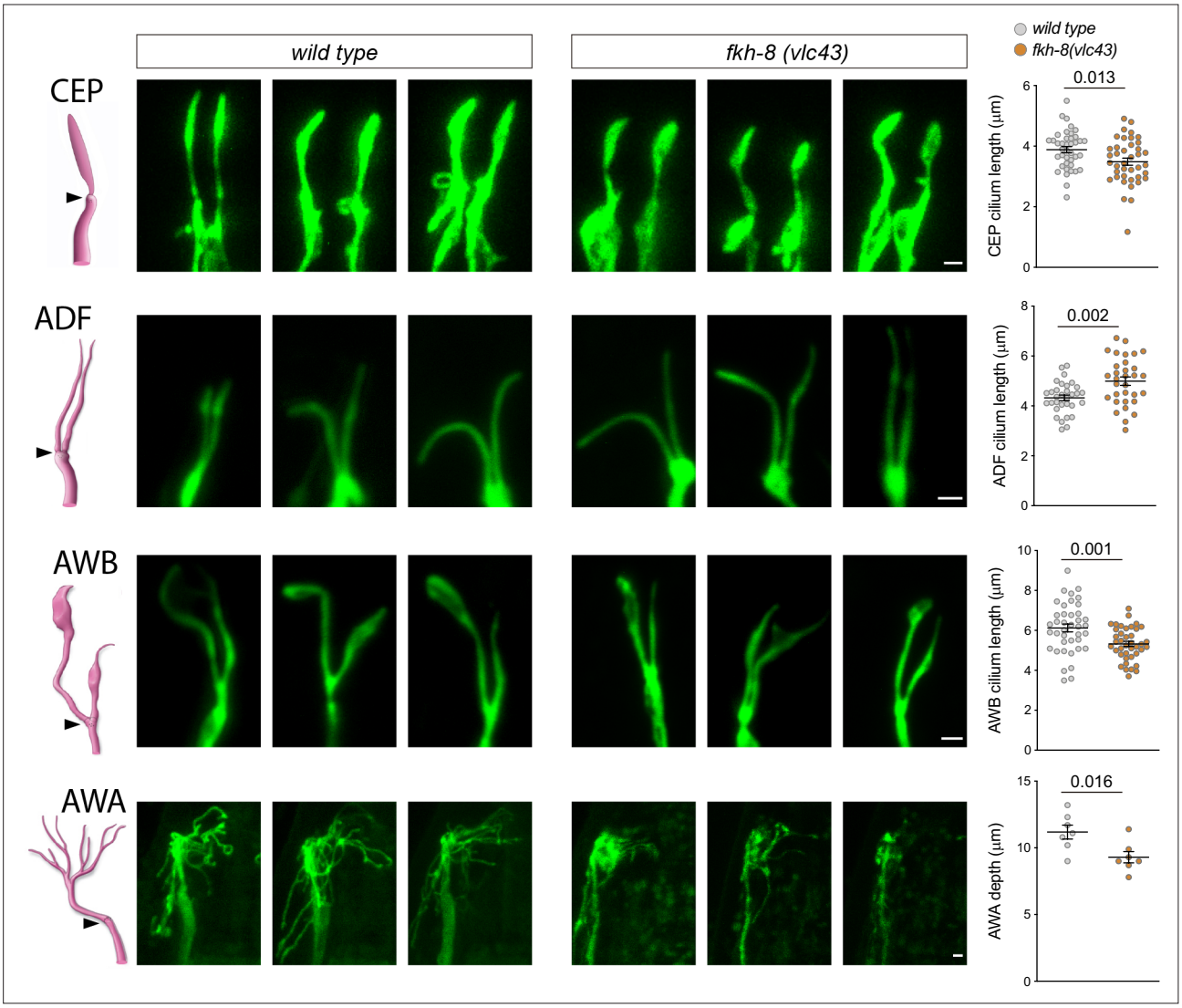

Figure 5. *fkh-8(vlc43)* null mutants display morphological defects in cilia. Integrated reporters unaffected in *fkh-8* mutant are used to label the cilia of several distinct subpopulations of ciliated neurons. CEP: *otIs259(dat-1::gfp)*; ADF: *zdIs13(tph-1::gfp)*; AWB: *kyIs104(str-1::gfp)*; AWA: *pkIs583(gpa-6::gfp)*. Panels show representative images from three animals in *wild type* and *fkh-8(vlc43)* mutant backgrounds. Cilium length of CEP and AWB neurons is significantly reduced in the absence of FKH-8 whereas ADF cilia length is increased. Depth of AWA cilium arborization is significantly reduced in *fkh-8(vlc43)* null mutants. Each dot in the graphs represents measures for a single cilium. Mean and standard error are represented. See ***Figure 5—figure supplement 1*** for cilia morphology analysis in worms immobilized in polystyrene beads and ***Figure 5—source data 1*** for raw data and statistics. CEP and AWB n=40; ADF n=32; AWA n=7.

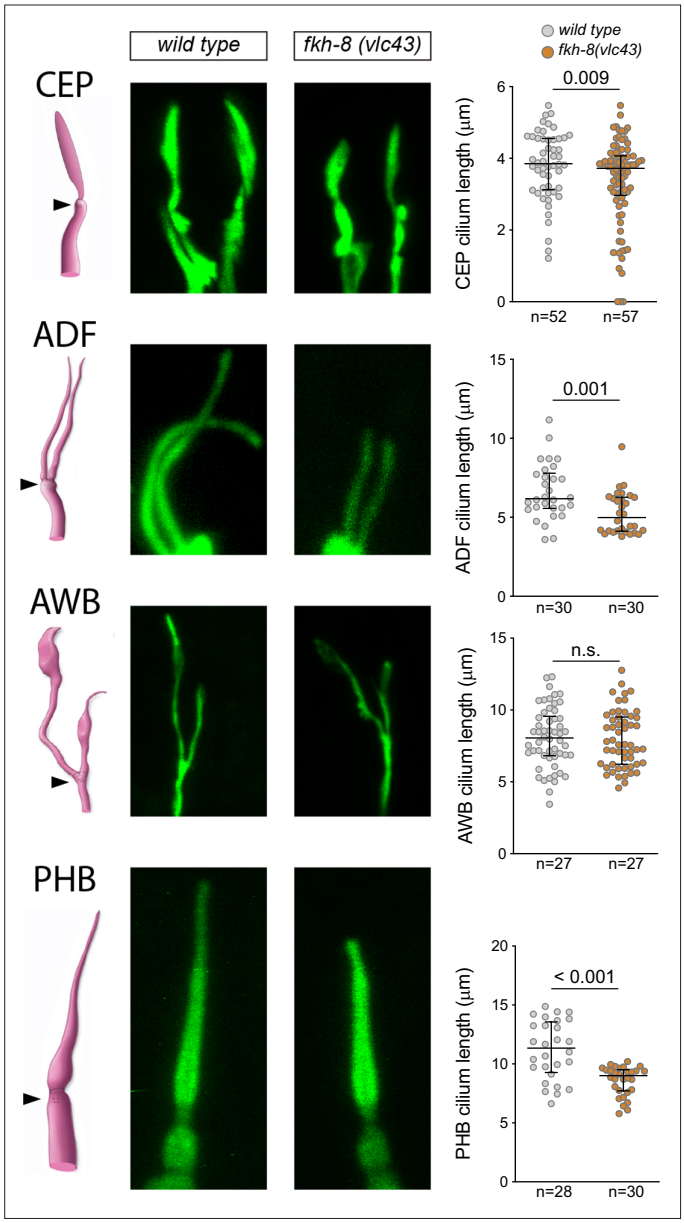

Figure 5—figure supplement 1. *fkh-8(vlc43)* null mutants display morphological defects in cilia using physical immobilization with polystyrene beads. Integrated reporters unaffected in *fkh-8* mutant are used to label the cilia of several distinct subpopulations of ciliated neurons. CEP: *otIs259(dat-1::gfp)*; ADF: *zdIs13(tph-1::gfp)*; AWB: *kyIs104(str-1::gfp)*; AWA: *pkIs583(gpa-6::gfp)*. Panels show representative images from *wild type* and *fkh-8(vlc43)* mutant backgrounds. Cilium length of CEP ADF and PHB is significantly reduced in the absence of FKH-8, whereas AWB cilia length is unaffected. Mean and standard error are represented. Please note that different fixation methods are used compared to ***Figure 5***. *CEP, AWB: n≥50, ADF: n≥30, PHB: n≥28.*

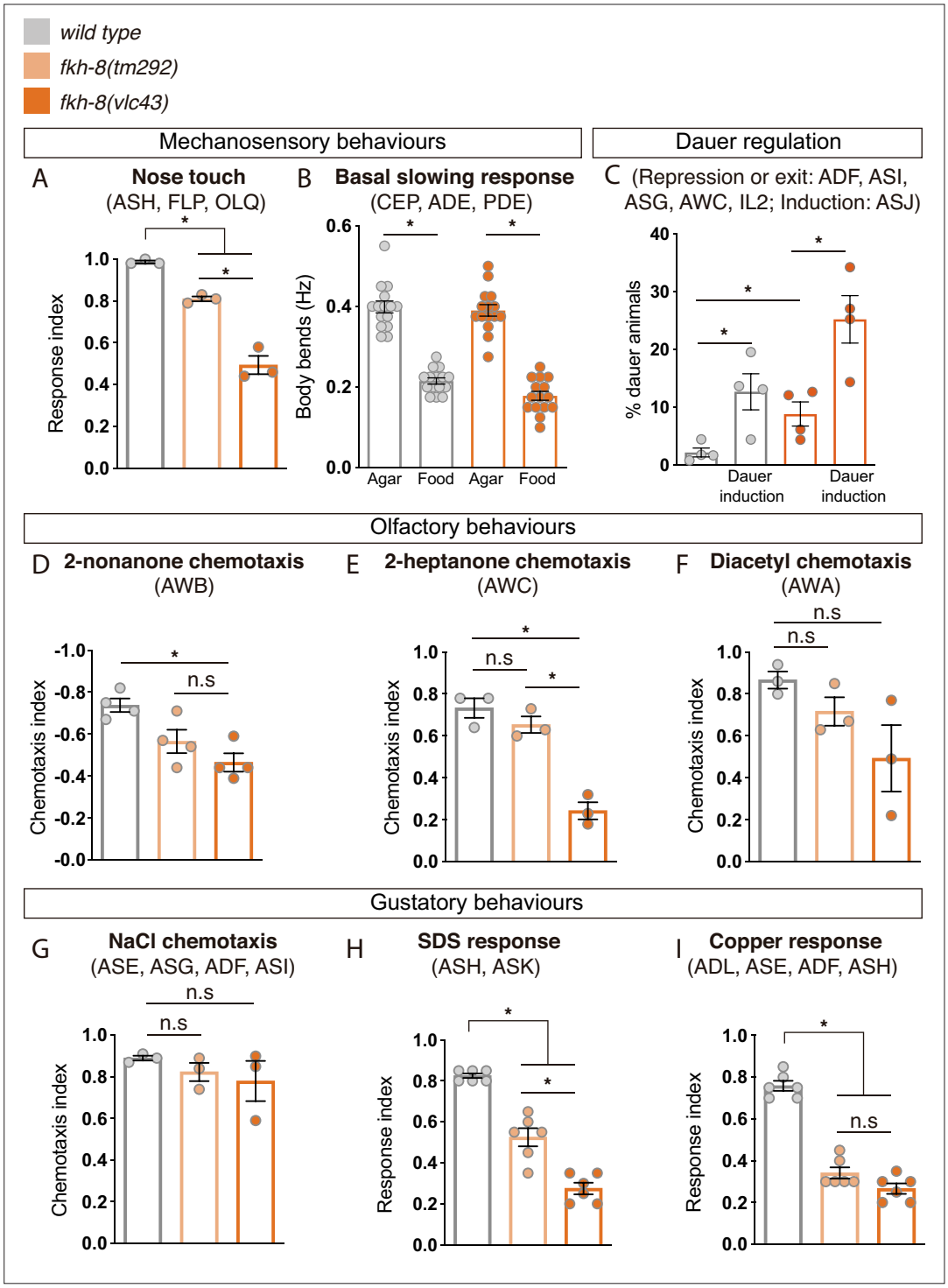

Figure 6. FKH-8 is required for the correct display of several sensory mediated behaviors. (**A**) Mutations in *fkh-8* significantly impair appropriate backward response to nose touch, revealing functionality defects for the ASH, FLP and/or OLQ ciliated neurons. This phenotype is stronger in *fkh-8(vlc43)* null mutants than in the hypomorphic *tm292* allele. n=20 animals per replicate, three biological replicates per genotype. (**B**) Decrease in locomotory rate upon re-entering a bacterial lawn is unaffected in *fkh-8* mutants. n=15 worms per genotype and condition. (**C**) *fkh-8* null mutants significantly fail to prevent *dauer* entry. Pheromones induce *dauer* in *fkh-8* mutants, albeit less efficiently than in controls. Four biological replicates n>295 per replicate and genotype. (D to F) Lack of *fkh-8* significantly impairs olfaction-mediated behaviors. Defects are observed for 2-nonanone repulsion mediated by AWB [*Wild type* n=59, 128, 114, 165; *fkh-8(tm292)* n=76, 123, 129, 209 and *fkh-8(vlc43)* n=82, 92, 130, 139] and

Figure 6 continued on next page

Figure 6 continued

2-heptanone attraction mediated by AWC neurons [*Wild type* n=124, 129, 133; *fkh-8(tm292)* n=68, 94, 102 and *fkh-8(vlc43)* n=87, 83, 85]. Diacetyl response, mediated by AWA, is affected but not to a significant level due to high variability in the response [*Wild type* n=168, 69, 103; *fkh-8(tm292)* n=57, 85, 110 and *fkh-8(vlc43)* n=115, 107, 74]. (G to I) Attractive chemotaxis towards NaCl is unaffected in *fkh-8* mutant animals. [*Wild type* n=62, 78, 72; *fkh-8(tm292)* n=105, 116, 106 and *fkh-8(vlc43)* n=111, 52, 78]. Avoidance behavior towards toxic SDS and copper anions is significantly impaired. [Six biological replicates, 5 worms per replicate and genotype, 4 tests per worm]. Mean and standard error are represented in all graphs. See ***Figure 6—figure supplement 1*** for quantification of non-cilia mediated behaviors and ***Figure 6—source data 1*** for raw data and statistics.

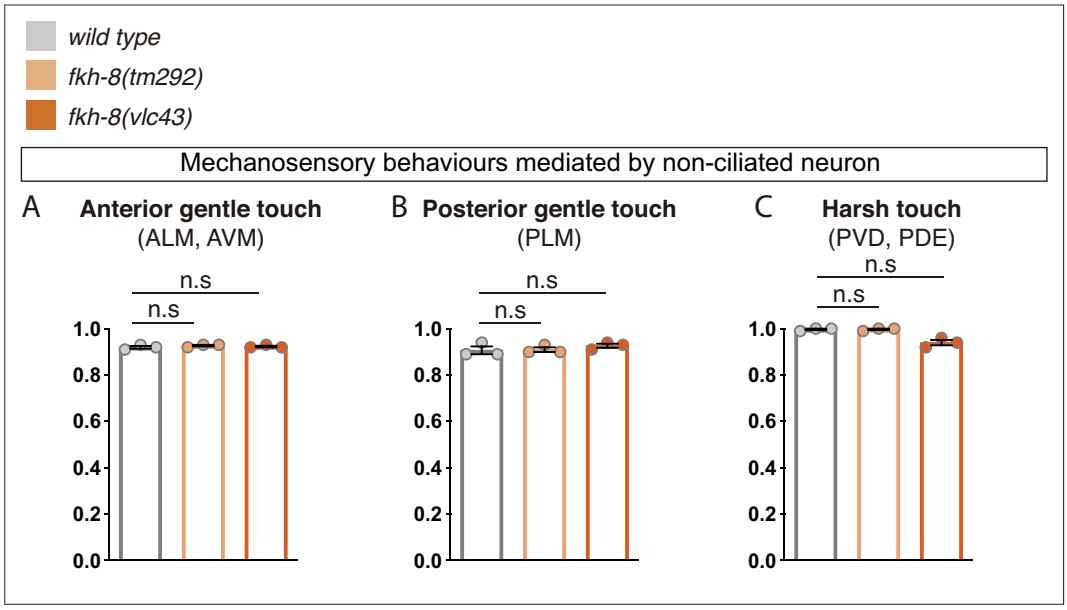

Figure 6—figure supplement 1. FKH-8 is not required for correct display of mechanosensory behaviors mediated by non-ciliated neurons. (**A** to **C**) *fkh-8* mutants show normal avoidance behaviors elicited by mechanical stimuli known as gentle touch and harsh touch paradigms, suggesting FKH-8 is not required for the correct functionality of non-ciliated neurons ALM, AVM, PLM, and PVD. Redundant actions of PVD and PDE controlling scape response to harsh touch prevent to assess defects about the functionality of ciliated PDE neurons. Mean and standard error for three independent replicates are represented. See ***Figure 6—source data 1*** for raw data. n=60 worms per genotype.

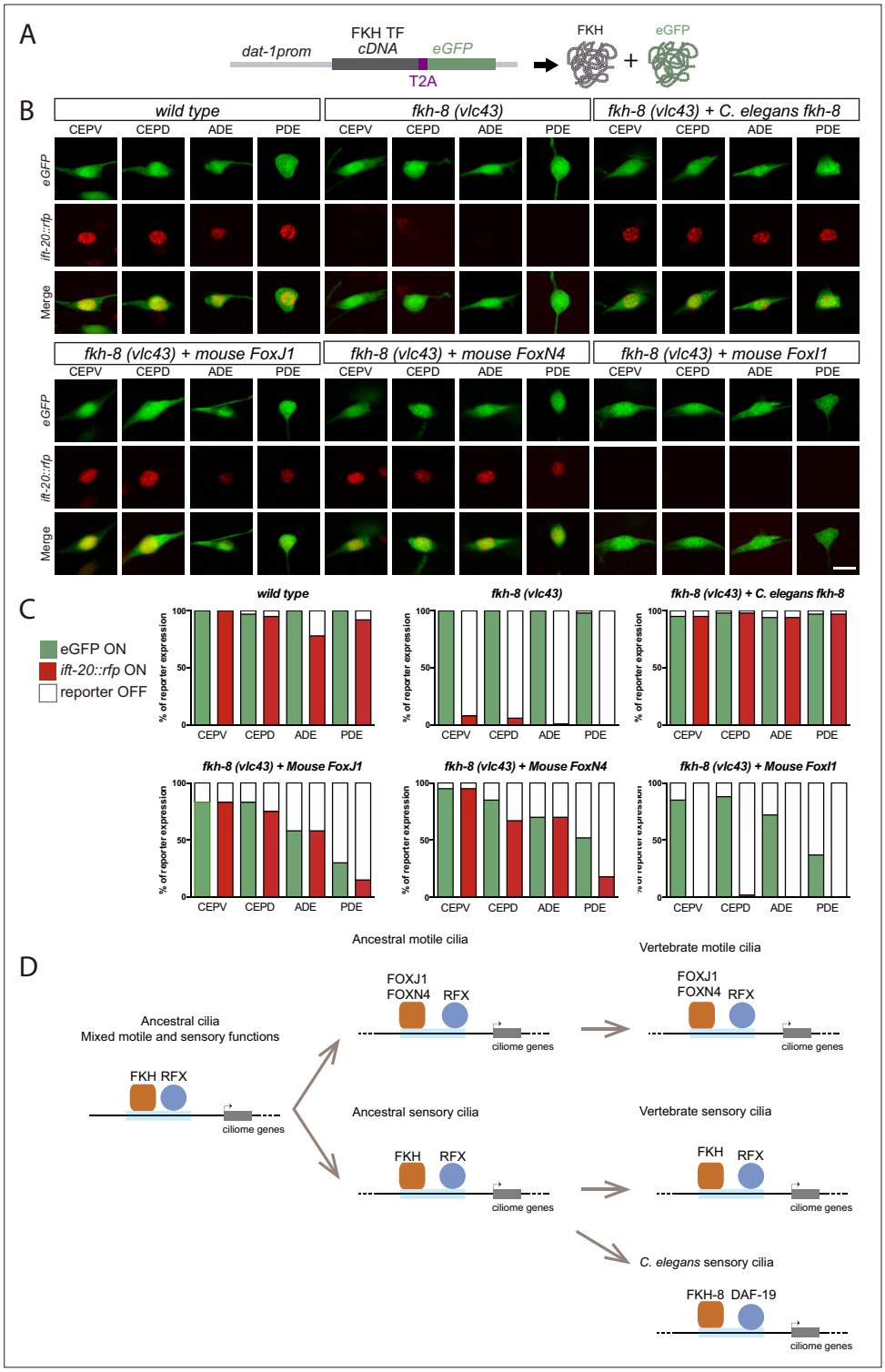

Figure 7. Mammalian FKH TFs with known motile cilia regulatory functions can rescue *fkh-8* mutant phenotype. (**A**) Rescue strategy: *dat-1* promoter, unaffected in *fkh-8* mutants, is used to drive FKH TF cDNA and eGFP expression specifically in the dopaminergic ciliated system. (**B**) Representative images of dopaminergic neurons expressing an integrated reporter for the core ciliome marker *ift-20* (in red) in *wild type*, *fkh-8(vlc43)* mutants and with the co-expression of different rescuing constructs. Scale bar = 5 µm. (**C**) Quantification of rescue experiments. *ift-20* reporter expression is lost from the dopaminergic neurons in *fkh-8(vlc43)* null mutants compared to *wild type* animals. Expression of FKH-8, FOXJ1, and FOXN4 but not FOXI1 is sufficient to recover *ift-20* expression in dopaminergic neurons. N=30 animals per transgenic line. See ***Figure 7—source data 1*** for raw data and

Figure 7 continued on next page

Figure 7 continued

similar results obtained with two additional transgenic lines per construct. (**D**) Speculative model on the evolution of ciliome gene regulatory logic. FKH and RFX TFs could have an ancestral role in the direct coregulation of ciliome genes before its functional diversification into motile and primary cilia cell types. Different RFX and FKH TF members could have evolved to regulate ciliome genes in specific cell types in different organisms. Orange squares represent FKH TFs and blue circles RFX TFs, light blue bars represent ciliome enhancers.